Soft Matter

PAPER

View Article Online
View Journal | View Issue

Cite this: *Soft Matter*, 2023, **19**, 2745

Toughening of poly(ionic liquid)-based ion gels with cellulose nanofibers as a sacrificial network†

Takaichi Watanabe,* Emiho Oe, Yuna Mizutani and Tsutomu Ono

Ion gels have the potential to be used in a broad range of applications, such as in carbon dioxide separation membranes and soft electronics. However, their low mechanical strength limits their practical applications. In this study, we developed double-network (DN) ion gels composed of TEMPO-oxidized cellulose nanofibers with hydrophobic groups (TOCNF) and cross-linked poly[1-ethyl-3-vinylimidazolium bis(trifluoromethanesulfonyl)imide] (PC_{2im}-TFSI) networks. The mechanical strength of the gel increased as the amount of TOCNF in the gels increased up to 6 wt%. Moreover, the fracture energy of the DN ion gels with 6 wt% TOCNF was found to be 19 times higher than that of the PC_{2im}-TFSI single network (SN) ion gels. Cyclic stress–strain measurements of the DN gels showed that the loading energy on the gels dissipates owing to the destruction of the physically cross-linked TOCNF network in the gels. The DN ion gels also exhibited a high decomposition temperature of approximately 400 °C because of the thermal stability of all components. Additionally, the fracture energy of the TOCNF/poly(ionic liquid) (PIL) DN ion gel was two times higher than that of the silica nanoparticles/PIL DN ion gel developed in our previous study [Watanabe *et al.*, *Soft Matter*, 2020, 16, 1572–1581]. This suggests that fiber-shaped nanomaterials are more effective than spherical nanomaterials in enhancing the mechanical properties of ion gels. These results show that TOCNF can be used to toughen PIL-based ion gels and hence broaden their applications.

Received 27th January 2023,
Accepted 22nd March 2023

DOI: 10.1039/d3sm00112a

rsc.li/soft-matter-journal

Introduction

Ion gels, which are composed of three-dimensional cross-linked polymer networks swollen with a large amount of ionic liquid (IL), have recently attracted significant attention as a new class of soft materials because of their unique properties such as high ionic conductivity,[1–5] thermal stability,[6,7] and electrochemical stability,[8,9] processability,[10,11] and handleability. These gels have potential applications in various fields, including as solid-state polyelectrolytes,[12,13] supercapacitors,[14,15] carbon dioxide separation membranes,[16–19] and as sensors and actuators[2,20,21] in soft electronics. However, their low mechanical strength hinders their practical use.

Over the past few decades, various strategies have been employed to improve the mechanical strength of ion gels, such as the use of homogeneous tetra-arm poly(ethylene glycol) networks[22,23] and self-assembled ABA-type triblock copolymers with IL-philic middle blocks and IL-phobic cross-linkable end blocks.[24,25] Recently, Tamate *et al.* developed the fabrication of highly stretchable and self-healing ion gels using ultra-high molecular weight polymers synthesized in an ionic liquid.[26,27] This approach does not use a chemical cross-linker in the gel, thereby achieving relatively high toughness and self-healing. Hu *et al.* fabricated tough and stretchable gels through the *in situ* random copolymerization of two monomers with different affinities for ionic liquids;[28] in this system, a polymer-rich phase with hydrogen bonds contributed to the energy dissipation, while an elastic solvent-rich phase withstood large strains, leading to gel toughening.

The double network (DN) concept, which has been widely successfully applied in hydrogels,[29–31] can also be effective in improving the toughness of ion gels. These gels comprise two interpenetrating networks: a rigid and brittle network and a soft and stretchable network; these two networks work together to dissipate the loading energy and maintain the integrity of the gel, respectively. Examples of DN ion gels include those made of chemically cross-linked poly(furfuryl methacrylate-*co*-methyl methacrylate) and physically cross-linked poly(vinylidene fluoride-*co*-hexafluoropropylene),[32] and those composed of poly(vinyl alcohol) and poly(vinylpyrrolidone).[33] Kamio *et al.* developed inorganic/organic DN and micro-double-network (μ-DN) ion gels using silica nanoparticles and poly(*N*,*N*-dimethylacrylamide).[34–37] In these gels, the inorganic silica nanoparticles form a partially clustered network in the IL *via* hydrogen bonding and van der

Department of Applied Chemistry, Graduate School of Natural Science, Okayama University, 3-1-1, Tsushima-naka, Kita-ku, Okayama, 700-8530, Japan. E-mail: wata-t@okayama-u.ac.jp, tono@okayama-u.ac.jp; Tel: +81-86-251-8072, +81-86-251-8083

† Electronic supplementary information (ESI) available. See DOI: https://doi.org/10.1039/d3sm00112a

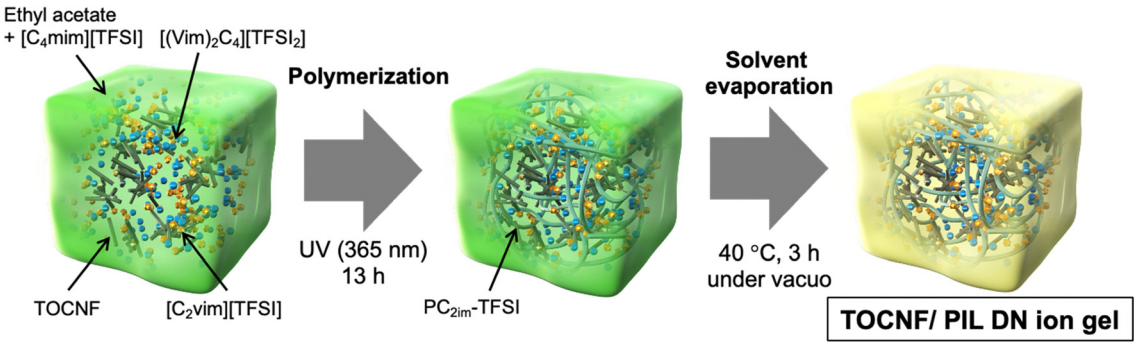

Scheme 1 Schematic illustration of the preparation of the TOCNF/PIL DN ion gel *via* photo-induced radical polymerization and subsequent solvent evaporation.

Waals interactions, and the loading energy is dissipated by the internal rupture of the silica nanoparticle network in the gels. In our previous study, we developed poly(ionic liquid) (PIL)-based DN ion gels composed of silica nanoparticles and PIL and examined the effect of the surface functionality of the silica nanoparticles on the mechanical strength of the ion gels.[38] We found that only pristine silica nanoparticles that contain hydroxide or silanol groups on the surface formed a partially clustered network in the IL and contributed to the toughening of the ion gels. This result suggests that nanomaterials with strong hydrogen bonding formation properties, such as cellulose and cellulose derivatives, could be effective in toughening ion gels.

In this study, we developed a new type of DN ion gel composed of physically cross-linked TEMPO-oxidized cellulose nanofibers with hydrophobic groups (TOCNF)[39] and chemically cross-linked poly[1-ethyl-3-vinylimidazolium bis(trifluoromethanesulfonyl)imide] (PC_{2im}-TFSI, PIL) networks with an ionic liquid (Scheme 1). TOCNF, a cellulose derivative known for its biocompatibility and ability to reinforce soft materials,[40–43] was expected to contribute to the formation of a physically cross-linked network in the IL[44] and improve the toughness of the ion gels through energy dissipation. To the best of our knowledge, this is the first study to report on the preparation of DN ion gels using TOCNF and PIL. The rheological behavior of TOCNF in the IL was examined to confirm the formation of a physically cross-linked TOCNF network. TOCNF/PIL DN ion gels with varying amounts of TOCNF and PIL single network (SN) ion gels were prepared, and their mechanical properties were compared with those of silica nanoparticles/PIL DN ion gels, which were previously reported by our group.[38] These ion gels were also subjected to cyclic tensile testing to evaluate their degree of energy dissipation. The differences in network structure between PIL SN and TOCNF/PIL DN gels were evaluated by SEM. Furthermore, the thermal stability and ionic conductivity of the ion gels was evaluated using thermogravimetric analysis and impedance analyzer, respectively.

Results and discussion

To determine whether TOCNF has the potential to cause gelation in an ionic liquid, an oscillatory shear measurement was performed using a TOCNF dispersion in [C_4mim][TFSI], as illustrated in Fig. 1(a). The elastic modulus (G') of the 3 wt% TOCNF dispersion in [C_4mim][TFSI] is significantly larger than its viscous modulus (G''); moreover G' is independent of the

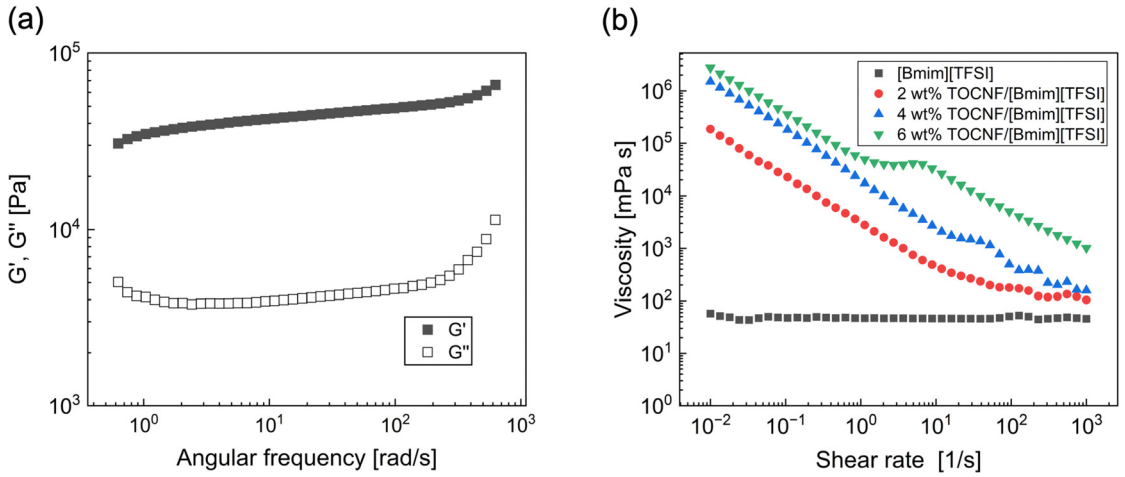

Fig. 1 (a) Elastic (G') and viscous (G'') moduli as a function of frequency for an IL dispersion with 3 wt% TOCNF. (b) Shear rate dependencies of viscosity for IL dispersions with different concentrations of TOCNF.

frequency across the measured range. This result indicates that the TOCNF dispersion acts as a soft solid-like material or gel, and that TOCNF is capable of physically cross-linking within [C_4mim][TFSI]. To further investigate the gelation of TOCNF in [C_4mim][TFSI], the viscosities of the [C_4mim][TFSI] and [C_4mim][TFSI] dispersions containing various concentrations of TOCNF were measured under different shear rates, as shown in Fig. 1b. The viscosity of pure [C_4mim][TFSI] was independent of the shear rate, which is consistent with previously reported literature values.[45] This observation suggests that pure [C_4mim][TFSI] behaves as a Newtonian fluid. In contrast, the viscosity of the TOCNF-containing dispersions decreased with increasing shear rate, up to 6 wt%. This shear-thinning behavior is probably caused by the rupturing of interfibrous physical bonds of TOCNF under shear, similar to what has been observed in dispersions of colloidal particles such as silica nanoparticles[46,47] and polysaccharides.[48] When a 6 wt% TOCNF dispersion was used, shear-thickening was also observed at shear rates between 1 and 10 [s^{-1}]. This indicates that TOCNF forms pseudo clusters at high concentration of TOCNF when shear is applied. Additionally, the zero-shear viscosity of the TOCNF-containing dispersions increased with increasing TOCNF concentration, indicating that the degree of interfibrous interactions and apparent cross-linking density of TOCNF in the ionic liquid can be enhanced by increasing the TOCNF concentration. However, when the concentration of TOCNF was increased to over 6 wt%, no significant change in the zero-shear viscosity was observed. This suggests that an excess amounts of TOCNF in [C_4mim][TFSI] is unlikely to contribute to network formation. Based on these findings, we expected that TOCNF may potentially improve the mechanical strength of PIL-based ion gels through the principle of energy dissipation.

PIL-based DN ion gels, comprising TOCNF and cross-linked PC_{2im}-TFSI, were fabricated by the photo-induced radical polymerization of [C_2vim][TFSI] in a mixture containing varying concentrations of TOCNF, [C_4mim][TFSI] (solvent), [$(Vim)_2C_4$]-[TFSI]$_2$ (cross-linker), Igragure® 2959 (photoinitiator), and ethyl acetate (solvent). Subsequently, ethyl acetate was removed using the solvent evaporation method. PIL SN ion gels were also prepared using a similar method, but without the inclusion of TOCNF. Fig. 2(a) and (b) show the photographs of a PIL SN ion gel and a TOCNF/PIL DN ion gel, respectively. Both ion gels appear transparent and self-standing, but are yellow in colour owing to the use of a cross-linker in their preparation. The PIL DN ion gels appear more yellow in color than the PIL SN ion gels because the TOCNFs scatter light. However, no macroscopic phase separation of TOCNF in the IL was observed, indicating that TOCNF was successfully incorporated into the ion gels.

To determine the mechanical strength of the TOCNF/PIL DN ion gels, uniaxial stretching experiments were conducted on ion gels containing various amounts of TOCNF (Fig. 3). The stress–strain curves for ion gels with different amounts of TOCNF are shown in Fig. 3(a). The results for the PIL SN ion gel composed of 50 wt% PC_{2im}-TFSI and 50 wt% [C_4mim][TFSI],

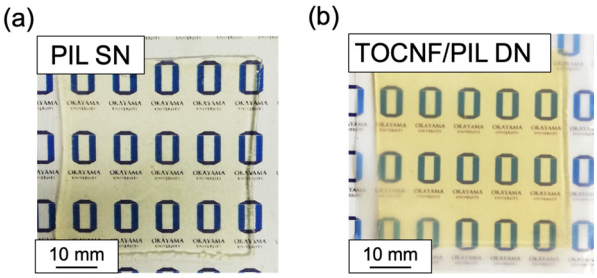

Fig. 2 Representative photographs of (a) PIL SN and (b) TOCNF/PIL DN ion gels, containing 50 wt% of [C_4mim][TFSI]. The amount of TOCNF in the DN ion gel was fixed at 6 wt%.

(*i.e.*, TOCNF concentration of 0 wt%) are also displayed. The mechanical strength of the TOCNF/PIL DN ion gel is higher than that of the PIL SN ion gel. Additionally, the mechanical strength of the TOCNF/PIL DN ion gels increased with increasing TOCNF concentration up to 6 wt%. These results demonstrate that the incorporation of TOCNF into the PIL-based ion gel enhances the mechanical properties of the ion gels. However, when the TOCNF content was 7 wt%, the fracture stress decreased. This could be due to the excess amount of TOCNF in the IL, which could have potentially hindered the extension of the PIL network upon stretching. Interestingly, the Young's modulus of the DN ion gel increased when the TOCNF concentration was increased up to 4 wt%. However, the Young's modulus did not significantly change when the TOCNF concentration was increased above 4 wt%. In contrast, the fracture stress of the DN gel increased up to 6 wt%. This result differs from that of the silica nanoparticle/PIL DN ion gel developed in our previous study.[38] The Young's modulus of the silica nanoparticle/PIL DN gel monotonically increased with increasing silica nanoparticle concentration, indicating that the dominant factor determining the mechanical properties of the TOCNF/PIL DN ion gels can change when the TOCNF amount is above 4 wt%. The mechanical properties, such as fracture strain, fracture stress, and fracture energy, are summarized in Fig. 3(b–d). The fracture strain and fracture stress of the TOCNF/PIL DN ion gel increased up to 5 wt% and 6 wt% TOCNF, respectively, and then exhibited a declining trend (Fig. 3b and c). Additionally, both the fracture strain and stress of the ion gels containing TOCNF were significantly higher than those without TOCNF. These results suggest that TOCNF does not act as a filler, but acts as a network to enhance both fracture strain and stress of the ion gel up to approximately 6 wt%. Moreover, the fracture energy of the DN ion gel, calculated from the area of the stress–strain curve, increased with increasing TOCNF concentration up to 6 wt% (Fig. 3d). From these results, we conclude that the incorporation of TOCNF into the PIL-based ion gel toughens the ion gel, and the optimal concentration of TOCNF in this system is 6 wt% relative to the polymer network.

SEM observation was then carried out to investigate differences in the microstructure of PIL SN and TOCNF/PIL DN ion gels. Fig. S3 (ESI†) shows the cross-sectional SEM images for lyophilized PIL SN and TOCNF/PIL DN gels after extraction of IL from the matrix. The microstructure of the PIL SN gel was a

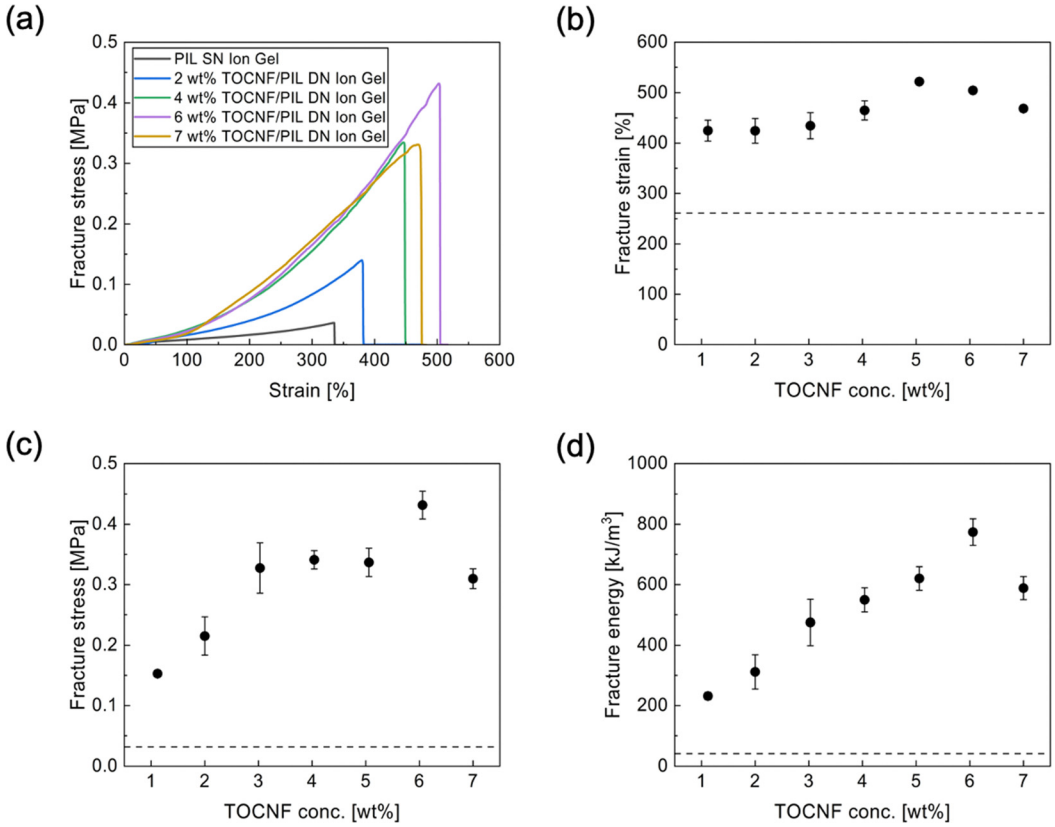

Fig. 3 Mechanical properties of DN ion gels composed of the TOCNF/PIL composite network (50 wt%) with various amounts of TOCNF and [C_4mim][TFSI] (50 wt%), and PIL SN ion gels composed of the PIL network (50 wt%) and [C_4mim][TFSI] (50 wt%). (a) Uniaxial tensile stress–strain curves of the DN with various TOCNF concentrations and SN ion gels, (b) fracture strain, (c) fracture stress, and (d) fracture energy. The dashed lines in each figure (b–d) indicate the value of the SN ion gel.

porous PIL network (Fig. S3a, ESI†), while that of the TOCNF/PIL DN gel was not only a porous PIL structure but also a TOCNF fibrous network and the TOCNF fibrous network was distributed throughout the PIL network (Fig. S3b, ESI†). It should be noted that these SEM images were taken after freeze-drying, and thus the domain sizes of the microstructure in the SEM images may differ from the as-prepared ion gels. However, SEM observation clearly shows that there are clear differences in the microstructure of PIL SN and TOCNF/PIL DN gels and that TOCNFs form a fibrous network in the DN gels.

Judging from the shear thinning behavior of TOCNF in IL (Fig. 1b), the network formation of TOCNF in the DN ion gels would be due to the formation of physical bonds based on strong attractive forces such as hydrophobic interaction and hydrogen bonding. To further confirm the physical network formation of TOCNF in the DN ion gel, the temperature dependence of G' of the DN ion gels was evaluated by oscillatory shear measurement at different temperatures (Fig. 4). The PIL SN ion gel showed a weak frequency dependence and a weak temperature dependence (Fig. 4a). On the other hand, the TOCNF/PIL DN ion gel showed strong frequency and temperature dependence (Fig. 4b). The G' decreased with increasing measurement temperature, indicating that the physical bonding between TOCNFs weakened with increasing temperature. These results strongly suggest that the physically cross-linked TOCNF fibrous network is formed before the PIL network is formed, and the TOCNF network could have physical adsorption to the PIL chains.

To confirm the toughening mechanism of the ion gel by introducing TOCNF, cyclic tensile stress loading–unloading experiments were conducted for the TOCNF/PIL DN and PIL SN ion gels, as shown in Fig. 5a and b, respectively. The TOCNF/PIL DN ion gel clearly showed a hysteresis loop in the cyclic stress–strain curves and softening behavior of the ion gel when the loading was applied (Fig. 5a), whereas the PIL SN ion gel did not (Fig. 5b). The hysteresis loop observed in the stress–strain curve of the TOCNF/PIL DN ion gel is derived from the partial deformation or destruction of the TOCNF network when the loading energy is applied on the gel, during which the PIL network can be stretched without critical crack formation that leads to the tearing of the gel. This result strongly implies that the toughening mechanism of the TOCNF/PIL DN ion gel is based on the energy dissipation derived from the disruption of the physically cross-linked TOCNF network when a large strain is induced.

To investigate the effect of the IL content on the mechanical properties of the TOCNF/PIL DN ion gels, the DN ion gels with various [C_4mim][TFSI] concentrations (50, 60, 70, 80 wt%) were prepared in the same manner as described above, and the uniaxial stretching experiments were performed. The concentrations of the

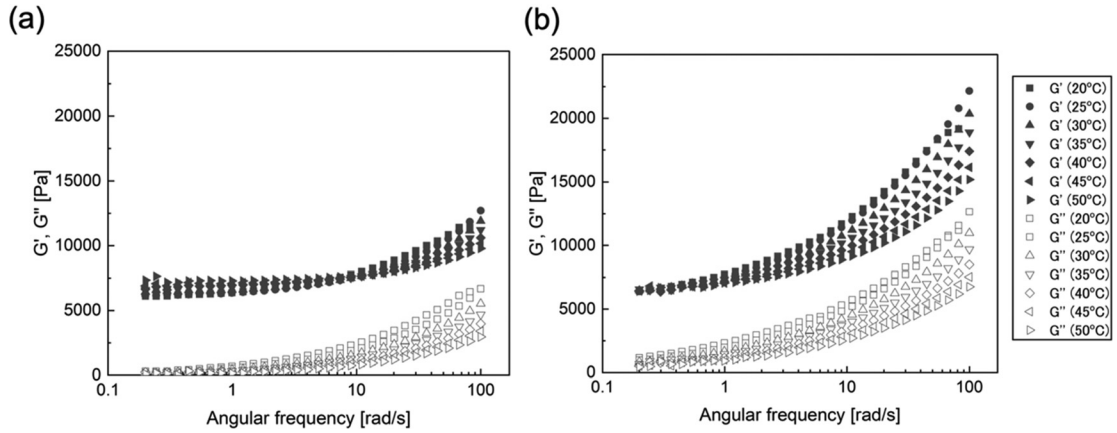

Fig. 4 Frequency dependence of storage modulus (G') and loss modulus (G'') of (a) PIL SN ion gel and (b) TOCNF/PIL DN ion gel measured at different temperatures. All ion gels had [C_4mim][TFSI] as IL. The IL content in the PIL SN and TOCNF/PIL DN ion gels was approximately 50 wt%. The TOCNF content in the TOCNF/PIL DN ion gels was 6 wt% relative to the PIL network.

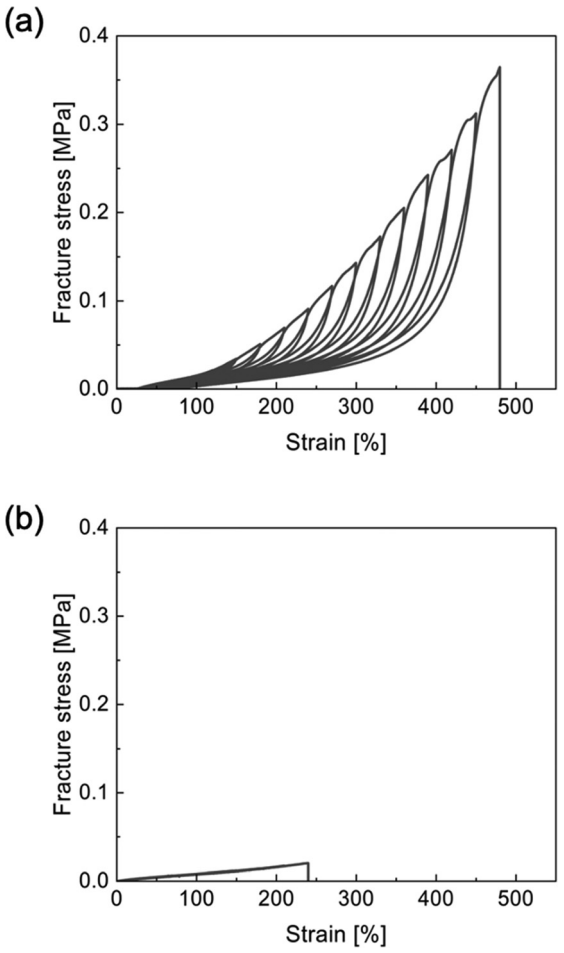

Fig. 5 Cyclic tensile stress–strain curves of (a) TOCNF/PIL DN ion gel and (b) PIL SN ion gel. The DN ion gel is composed of the TOCNF/PIL composite network (50 wt%) and [C_4mim][TFSI] (50 wt%), and the PIL SN ion gel is composed of the PIL network (50 wt%) and [C_4mim][TFSI] (50 wt%).

cross-linker and TOCNF relative to the polymer component were fixed at 0.75 mol% and 6 wt%, respectively, based on the results of our preliminary uniaxial stretching experiments. As shown in Fig. 6a, the fracture stress of the DN ion gel decreased as the IL content increased from 50 to 80 wt%, while the fracture strain increased. The reduction in the mechanical properties of the DN ion gels was caused by the decrease in the amount of the PIL network in the ion gels. Although the DN ion gel with 80 wt% IL showed the weakest with the fracture stress of approximately 50 kPa, the gel was self-standing, and leakage of the IL from the gel was not observed. Fig. 6b–d show the cyclic tensile stress loading–unloading curves of the DN ion gels with various amounts of IL. The DN ion gels clearly show hysteresis loops in the cyclic stress–strain curves, regardless of the IL content in the gels. This result indicates that the TOCNF network can be formed in the ion gel and it contributes to energy dissipation to toughen the ion gels.

PIL-based ion gels exhibit high thermal stability because all the components of the ion gel have high thermal stability. To investigate the thermal stability of the PIL-based DN ion gels, thermogravimetric analysis was conducted for the PIL SN and TOCNF/PIL DN ion gels (Fig. 7). The decomposition temperatures (T_{d10}) of the PIL SN and TOCNF/PIL DN ion gels were 399 °C and 391 °C, respectively. Although the introduction of TOCNF in the PIL-based ion gel slightly decreased the T_{d10}, the value was higher than that of the previously reported ion gels.[49]

To evaluate the effect of TOCNF on the ionic conductivity of the gels, the ionic conductivity of PIL SN and 6 wt% TOCNF/PIL DN ion gels with 50 wt% IL content was investigated by impedance analyzer. PIL SN ion gel and 6 wt% TOCNF/PIL DN ion gel showed the same level of ionic conductivity with 1.63×10^{-4} and 1.45×10^{-4} S cm^{-1} at 20 °C, respectively. This result indicates that the addition of TOCNF to PIL ion gels would not affect the conductivity. However, these values were approximately one order of magnitude lower than that of the pure [C_4mim][TFSI] (2.30×10^{-3} S cm^{-1} at 20 °C). This may be due to the increase in IL viscosity in the gels, resulting in high electrical resistance. In order to increase the ionic conductivity for the ion gels with and without TOCNF, the next step will be to properly select IL species with high ionic conductivity and increase the IL content while maintaining the toughness of the gels.

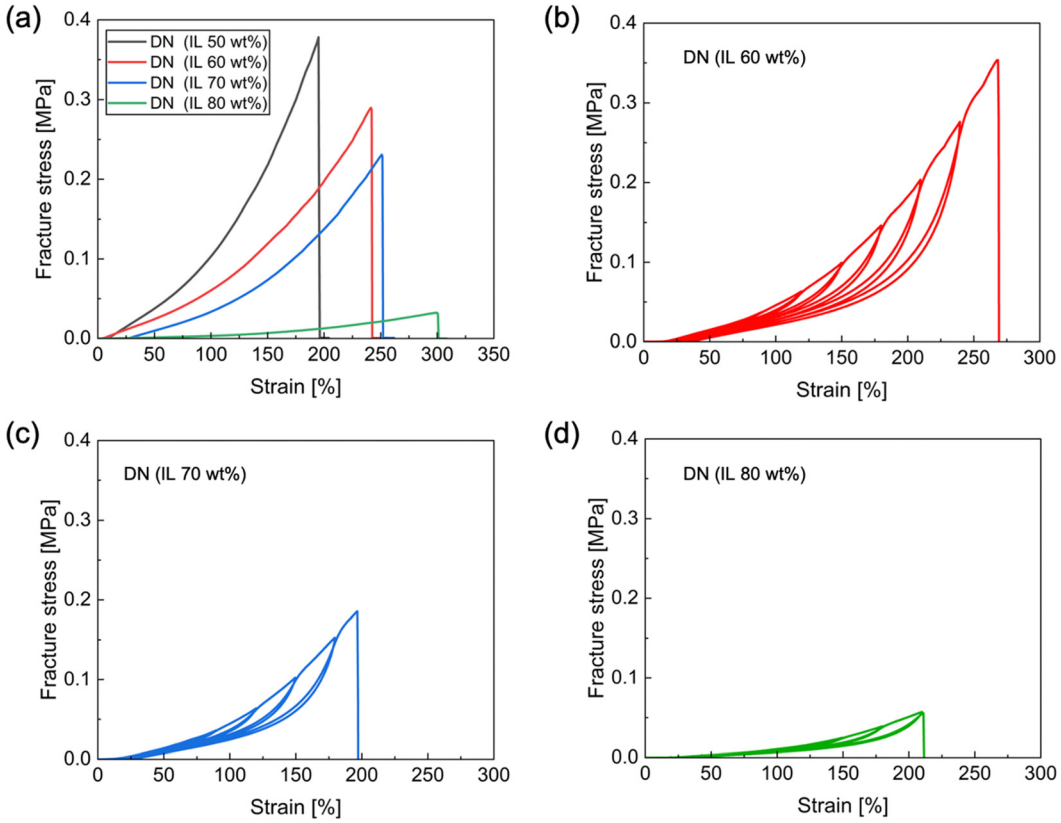

Fig. 6 Mechanical properties of the DN ion gels with various amounts of [C_4mim][TFSI]. The concentrations of the cross-linker and TOCNF are fixed at 0.75 mol% and 6 wt% relative to polymer concentration, respectively. (a) Uniaxial tensile stress–strain curves of the DN gels with various IL contents, and (b–d) cyclic tensile stress–strain curves of the DN ion gels.

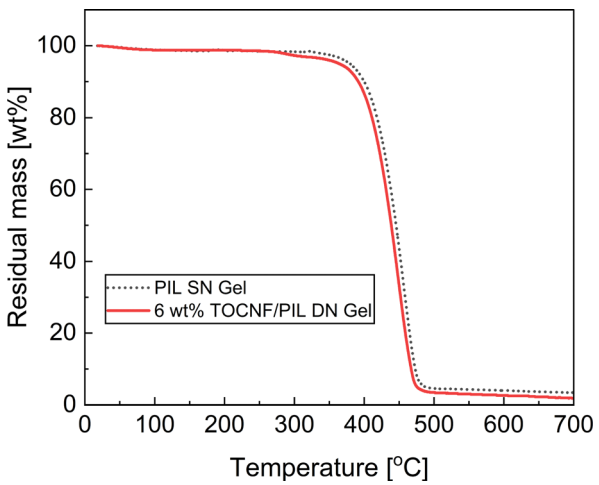

Fig. 7 Thermogravimetric analysis curves of the TOCNF/PIL DN ion gel and PIL SN ion gel. The IL contents in both gels were 50 wt%.

In our previous study, we have demonstrated that the addition of fumed silica nanoparticles (silica NPs) into a PIL-based ion gel enhanced its mechanical properties through the formation of a DN.[38] This toughening mechanism is based on energy dissipation through the rupture of a partially clustered silica NP network upon the application of loading energy; this mechanism is similar to the toughening mechanism of the TOCNF/PIL DN ion gel as discussed above. In this study, we compared the mechanical properties of the TOCNF/PIL DN ion gel and the silica NP/PIL DN ion gel. Fig. 8a shows the stress–strain curves of the TOCNF/PIL DN ion gel, silica NP/PIL DN ion gel, and PIL SN ion gel. The TOCNF/PIL DN ion gel exhibited approximately two times higher fracture stress than the silica NP/PIL DN ion gel, while their fracture strain was almost the same (500%). Therefore, the fracture energy of the TOCNF/PIL DN ion gel (773 ± 43 kJ m^{-3}) was approximately two times higher than that of the silica NP/PIL DN ion gel (390 ± 53 kJ m^{-3}). These results indicate that there are no significant differences between the stretchability and Young's moduli of the TOCNF/PIL and silica NP/PIL DN ion gels, and that similar cross-linked PIL networks can be formed in both ion gels. The main difference in the mechanical properties of the DN ion gels is the increase in stress when the strain increases. This observation indicates that there may be a difference in the degree of energy dissipation through the destruction of the physically cross-linked nanomaterial network. To estimate the difference in the degree of energy dissipation by the nanomaterial networks in the DN ion gels, we calculated the dissipated energy per cycle in the cyclic stress loading–unloading experiments for the TOCNF/PIL DN ion gels and silica NP/PIL DN ion gels from the area of each hysteresis

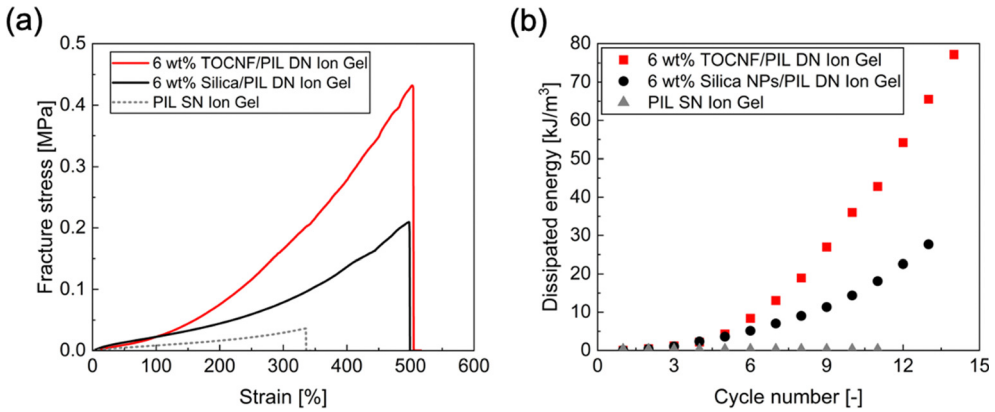

Fig. 8 Comparison of the mechanical properties of the TOCNF/PIL DN ion gel, silica NP/PIL DN ion gel, and PIL SN ion gel. The concentration of the nanomaterial is fixed at 6 wt% relative to the polymer network. (a) Uniaxial tensile stress–strain curves, (b) dissipated energy as a function of cycle number during the cyclic tensile measurements.

loop cycle, as shown in Fig. 8b. In both DN ion gels, the amount of energy dissipated increased with increasing number of cycles. Moreover, the TOCNF/PIL DN ion gel dissipated more energy per cycle than the silica NP/PIL DN ion gel when the same amount of strain was applied to the gels. This may have occurred due to the high network density of TOCNF. We assumed that fiber-shaped TOCNFs (aspect ratio $>$ 30) interact more easily with each other than sphere-shaped silica NPs (aspect ratio $\sim$ 1), leading to the larger apparent cross-linking density of the TOCNF network compared to the silica NP network. When a loading energy is applied, the TOCNF network in the ion gel can be destroyed more easily than silica NP network, while maintaining the PIL network without breakage. This increases the energy dissipation and fracture stress. This indicates that fiber-shaped nanomaterials are more effective for toughening the ion gels as sacrificial networks than sphere-shaped nanomaterials. However, the various interactions among nanomaterials, ILs, and PIL networks need to be quantitatively analyzed in future studies.

The toughening of ion gels is a major topic in the field and has therefore received considerable attention over the last few decades. The most common approach to toughening ion gels is by analogy with hydrogels. For example, Fujii *et al.* developed ion gels with conductivity as high as pure IL by using much lower concentrations of a homogeneous tetra-PEG network (3–6 wt%).[22] In addition, Tang *et al.* developed DN ion gels consisting of a chemically cross-linked polymer network and a physically cross-linked polymer network, which exhibited high toughness, self-healing ability and relatively high ionic conductivity.[32] Kamio *et al.* proposed DN ion gels composed of a physically cross-linked silica nanoparticle (nanomaterial) network and a chemically cross-linked polymer network,[34] and recently developed tough ion gels by incorporating zeolitic imidazole framework-8 (ZIF-8) nanoparticles into a poly(*N*,*N*-dimethylacrylamide)-based polymer network. ZIF-8 nanoparticles serve as multifunctional reversible crosslinkers, imparting toughness and self-healing properties to the gels.[50] In this study, we reported TOCNF/PIL DN ion gels, which belong to the nanomaterial/polymer DN ion gel series and can be easily prepared by adding nanomaterial to the sol solution. These gels exhibited excellent thermal stability and higher toughness than silica nanoparticle/PIL DN ion gels previously reported by our group.[38] Although it is difficult to make a fair comparison of the properties of ion gels such as toughness, ionic conductivity, and CO_2 separation due to their sensitivity to compositional variables such as IL species, IL content and viscoelastic properties, our results show that introducing fiber-shaped nanomaterial into ion gels as the first network can be an effective method of toughening as it induces large energy dissipation. Depending on the task-specific application of the gels, further fine-tuning of their chemical composition may be required.

Conclusions

We demonstrated that the incorporation of TOCNF in a PIL-based ion gel enhances its mechanical properties through the formation of a DN. Uniaxial stretching experiments showed that the fracture energy of the TOCNF/PIL DN ion gel was 19 times higher than that of the PIL SN ion gel (without TOCNF). Moreover, the fracture energy increased as the TOCNF concentration in the ion gel increased up to 6 wt%. Cyclic stress loading–unloading experiments of the TOCNF/PIL DN ion gel clearly showed a hysteresis loop, indicating that the toughening mechanism involves energy dissipation. The physically cross-linked TOCNF network can be preferentially destroyed when a loading energy is applied on the gel, during which the chemically cross-linked PIL network is stretched without breaking the gel. This toughening mechanism is similar to that of the silica NP/PIL DN ion gel, which was developed in our previous study. However, the toughness of the TOCNF/PIL DN ion gel was two times larger than that of the silica NP/PIL DN ion gel. This may be due to the fiber-shaped structure of the TOCNFs, which can easily interact with each other and dissipate more energy than spherical silica NPs. These findings suggest that the incorporation of TOCNF into the PIL-based ion gels can effectively improve their mechanical properties. Consequently, these tough ion gels

can be applied in carbon dioxide separation membranes and soft electronics such as polyelectrolytes, sensors, and actuators.

Experimental section

Materials

A 7.8 wt% dispersion of TEMPO-oxidized cellulose nanofiber with hydrophobic groups (TOCNF) in ethyl acetate was kindly provided by Nippon Paper Industries Co., Ltd. The diameter and length of the TOCNF were 32.5 ± 5.8 nm and larger than 1 μm, respectively. 1-Butyl-3-methylimidazolium bis(trifluoromethanesulfonyl)imide ([C_4mim][TFSI]) and 1-ethyl-3-vinylimidazolium bis(trifluoromethanesulfonyl)imide ([C_2vim][TFSI]) were purchased from FUJIFILM Wako Pure Chemical Corp. (Osaka, Japan) and used as received. In addition, 1-vinylimidazole and 1,4-dibromobutane were also purchased from FUJIFILM Wako Pure Chemical Corp. (Osaka, Japan) and used without further purification. Ethanol, diethyl ether, and lithium bis(trifluoromethanesulfonyl)imide (LiTFSI) were purchased from FUJIFILM Wako Pure Chemical Corp. (Osaka, Japan) and used as received. Furthermore, 2-Hydroxy-4′-(2-hydroxyethoxy)-2-methylpropiophenone (Ciba® IRGACURE® 2959), which was purchased from Ciba Specialty Chemicals (Switzerland), was used as a photoinitiator to synthesize the PC_{2im}-TFSI network in an IL. The deionized water used in all experiments was produced using an Elix UV purification system (Millipore, Japan). The chemical structures of [C_4mim][TFSI], [C_2vim][TFSI], Ciba® IRGACURE® 2959, [$(Vim)_2C_4$]Br_2, and [$(Vim)_2C_4$][Tf_2N]$_2$ are shown in Fig. S1 (ESI†).

Synthesis of 1,4-bis(3-vinylimidazolium-1-yl) butane bis(trifluoromethanesulfonyl)imide [$(Vim)_2C_4$][TFSI]$_2$ as a cross-linking reagent containing ionic liquid groups

A cross-linking reagent, [$(Vim)_2C_4$][TFSI]$_2$, containing ionic liquid groups, was synthesized by reacting 1-vinylimidazole with 1,4-dibromobutane, followed by an anion exchange reaction with LiTFSI (as shown in Scheme S1, ESI†) In this process, 1-vinylimidazole (0.10 mol, 9.1 mL) was mixed with ethanol (7.5 mL) in a round-bottom flask (150 mL) that had been dried and purged with argon. Subsequently, 1,4-dibromobutane (0.055 mol, 6.8 mL) was added dropwise to the flask and the mixture was stirred at 70 °C under an argon atmosphere for 24 h. The reaction mixture was then precipitated in ethyl acetate (200 mL) three times to remove any unreacted reagents. The purified product was dried at 50 °C under reduced pressure overnight, yielding 20.1 g of [$(Vim)_2C_4$]Br_2 in 99% yield, as shown in the proton nuclear magnetic resonance (^{1}H NMR) spectrum in Fig. S2a (ESI†). The anion exchange reaction of [$(Vim)_2C_4$]Br_2 with LiTFSI was then performed by mixing 60 mL of an aqueous solution containing [$(Vim)_2C_4$]Br_2 (7.5 mmol, 3.03 g) with 60 mL of an aqueous solution containing LiTFSI (16.5 mmol, 4.74 g). The resultant mixture was stirred at room temperature for 24 h under an argon atmosphere to exchange the Br_2 counter anion with the [TFSI]$_2$ anions. The resulting [$(Vim)_2C_4$][TFSI]$_2$ was washed three times with pure water (100 mL) and freeze dried for 24 h to remove any residual salt. The product yield of [$(Vim)_2C_4$][TFSI]$_2$ was 4.2 g (69.5%), as shown in the ^{1}H NMR spectrum in Fig. S2b (ESI†). The successful anion exchange from Br to TFSI was confirmed by peak shifting from a′ (9.46 ppm, 2H in Fig. S2b, ESI†) to a (9.40 ppm, 2H in Fig. S2a, ESI†).

Preparation of TOCNF/PIL DN ion gels

The TOCNF/PILs DN ion gels were prepared *via* the photopolymerization of an ionic monomer ([C_2vim][TFSI]) in the presence of an ionic liquid ([C_4mim][TFSI]), ethyl acetate, and TOCNF/ethyl acetate dispersion. Ethyl acetate was then removed by vacuum drying at 40 °C. The typical experimental procedure for the preparation of the TOCNF/PIL DN ion gel is described as follows. First, a 4.7 wt% TOCNF dispersion in ethyl acetate was dried at 40 °C under reduced pressure for 1 hour to prepare a 15.1 wt% TOCNF dispersion in ethyl acetate. The 15.1 wt% TOCNF dispersion (1.013 g) was then mixed with [C_4mim][TFSI] (3.5 g) using a vortex mixer for 1 h to obtain a homogeneous TOCNF dispersion, followed by drying at 40 °C under reduced pressure for 1 h to remove excess ethyl acetate. Next, [C_2vim][TFSI] (3.0 g), [$(Vim)_2C_4$][TFSI]$_2$ (0.021 g), and Irgacure 2959 (0.0016 g) were added, and mixed using a vortex mixer, and stirred to prepare the precursor solution. The precursor solution was injected into a mold composed of two glass plates with an FEP film and a PTFE spacer with 1 mm thickness and was irradiated with 365 nm UV light for 13 h (1820 μW cm^{-2}). The product was dried *in vacuo* at 40 °C for more than 3 h. The IL content after drying was fixed at 50 wt%.

Mechanical property measurement of ion gels

The mechanical properties of the ion gels were evaluated using an automatic recording universal testing instrument (EZ Test EZ-SX 500 N, Shimadzu Co., Japan) at 25 °C. To conduct the stretching test, dumbbell-shaped specimens with lengths, widths, and thicknesses of 35, 2, and 1.0 mm, respectively, were used. The fabricated sample was attached to the instrument at 15 mm between the jigs. The uniaxial stretching test was conducted by stretching the sample at a constant strain rate of 50 mm min^{-1}. The stress–strain curves were recorded automatically until the specimens were broken. The fracture stress, fracture strain and fracture energy of the ion gels were obtained as the mean values of the measurements in triplicate for each sample. In the cyclic tensile test, the loading and unloading operations were performed, and the stress–strain curves were recorded until the sample broke, while gradually increasing the stretching strain in intervals of 0.3.

Rheological measurement of TOCNF/[C_4mim][TFSI] dispersion

A TOCNF dispersion in ethyl acetate (4.71 wt%) was dried *in vacuo* at 40 °C for 1 h to remove the excess ethyl acetate, which afforded a 14.7 wt% TOCNF dispersion in ethyl acetate. The TOCNF dispersion was then mixed with [C_4mim][TFSI] using a vortex mixer for 1 h to obtain a homogeneous TOCNF/[C_4mim][TFSI] dispersion. The dynamic frequency sweep and viscosity measurements of the TOCNF/[C_4mim][TFSI] dispersion were performed using a rheometer (MCR302, Anton Paar,

Japan). The viscosity dependence of the shear of the TOCNF/[C_4mim][TFSI] dispersion as a sample was evaluated using a rheometer with a parallel-plate geometry (PP50; diameter = 50 mm, gap = 0.3 mm) at 25 °C. A similar measurement was conducted using [C_4mim][TFSI] as the control. After pre-shearing the samples at 1000 s^{-1} for 60 s, the change in the viscosity of the solution was measured as a function of the shear rate from 1000 to 0.01 s^{-1}. Dynamic frequency sweep measurements of the TOCNF/[C_4mim][TFSI] dispersion were performed with a parallel-plate geometry (PP25; diameter = 25 mm, gap = 0.3 mm). The measurements were performed in the angular frequency range of 0.6–628 rad s^{-1} at 20 °C and strain level of 0.1%, respectively. The temperature dependence of the viscoelastic behavior of the gels was measured with a parallel-plate geometry (PP25; diameter = 25 mm, gap = 0.1 mm) in the angular frequency range of 0.1–1000 rad s^{-1} at different temperatures ranging from 20 to 50 °C in 5 °C increments, with a strain level of 1%.

Thermal gravimetric (TG) measurements of the samples

TG measurements of the samples were conducted using open Al pans on a thermogravimetry/differential thermal analyzer (DTG-60, Shimadzu, Japan) from 25 to 600 °C at a heating rate of 10 °C min^{-1} under a nitrogen atmosphere. The weight of each sample was fixed at 5 mg. The DN ion gel samples were heated from room temperature to 700 °C at a heating rate of 10 °C min^{-1} under a nitrogen atmosphere.

SEM observation of the samples

The morphology of the samples was observed with a field emission scanning electron microscope (SEM, S-4700, Hitachi Ltd., Japan) at a voltage intensity of 2 kV. Prior to observation, a small piece of ion gel was washed three times with acetone to remove IL and then immersed in a large amount of *tert*-butyl alcohol. The sample dispersion was then freeze-dried overnight. The lyophilized sample was cut with a blade and then sputter-coated (E-1030 Ion-Sputter, Hitachi Ltd., Japan) with Pd/Pt for 1 min to reduce the sample charge. The cut surface was observed with SEM.

Ionic conductivity measurements of the samples

The ionic conductivity of the gel films was measured by the impedance analyzer using LCR meter (IM3536, Hioki, Japan) in the frequency range 4 Hz –10 MHz. The ionic conductivity (σ [mS cm^{-1}]) was then calculated as $\sigma = l/(Ra)$, where l is the sample thickness [cm], a is the surface area of the sample [cm^2], and R is the bulk resistance determined from the real part of the impedance, Z', in the high-frequency plateau [Ω].

Author contributions

T. W., E. O., Y. M., and T. O. designed the experiments. T. W., E. O. and Y. M. performed the experiments and analyzed the data. T. W., E. O., Y. M., and T. O. interpreted the results and wrote the manuscript. T. W. and T. O designed the research.

Conflicts of interest

There are no conflicts to declare.

Acknowledgements

This work was partly supported by the JSPS KAKENHI (grant numbers: JP20KK0325 and JP21H04629) and the New Energy and Industrial Technology Development Organization (NEDO) (grant number: JPNP20004). We also thank Nippon Paper Industries Co., Ltd. (Japan) for supplying the TOCNF dispersion in ethyl acetate.

References

1 S. Zhang, K. H. Lee, J. Sun, C. D. Frisbie and T. P. Lodge, *Macromolecules*, 2011, **44**, 8981–8989.
2 Y. J. Son, J. W. Bae, H. J. Lee, S. Bae, S. Baik, K.-Y. Chun and C.-S. Han, *J. Mater. Chem. A*, 2020, **8**, 6013–6021.
3 K. Shahzadi, W. Xiong, M. Shekh, F. J. Stadler and Z.-C. Yan, *ACS Appl. Mater. Interfaces*, 2020, **12**, 49050–49060.
4 B. Tang, S. P. White, C. D. Frisbie and T. P. Lodge, *Macromolecules*, 2015, **48**, 4942–4950.
5 T. Fukushima, A. Kosaka, Y. Ishimura, T. Yamamoto, T. Takigawa, N. Ishii and T. Aida, *Science*, 2003, **300**, 2072–2074.
6 Y. Wang, Y. Chen, J. Gao, H. G. Yoon, L. Jin, M. Forsyth, T. J. Dingemans and L. A. Madsen, *Adv. Mater.*, 2016, **28**, 2571–2578.
7 M. Que, Y. Tong, G. Wei, K. Yuan, J. Wei, Y. Jiang, H. Zhu and Y. Chen, *J. Mater. Chem. A*, 2016, **4**, 14132–14140.
8 B. Huang, Y. Zhang, M. Que, Y. Xiao, Y. Jiang, K. Yuan and Y. Chen, *RSC Adv.*, 2017, **7**, 54391–54398.
9 T. Ueki, R. Usui, Y. Kitazawa, T. P. Lodge and M. Watanabe, *Macromolecules*, 2015, **48**, 5928–5933.
10 Y. Isano, H. Fujita, K. Murakami, S. Ni, Y. Kurotaki, T. Takano, Y. Isoda, R. Matsuda, F. Nakamura, Y. Nishitai, N. Ochirkhuyag, K. Inoue, H. Kawakami, Y. Okubo, K. Ueno, T. Fujie and H. Ota, *Adv. Mater. Technol.*, 2022, **7**, 2200209.
11 B. Tang, D. K. Schneiderman, F. Zare Bidoky, C. D. Frisbie and T. P. Lodge, *ACS Macro Lett.*, 2017, **6**, 1083–1088.
12 L. Yu, L. Yu, Q. Liu, T. Meng, S. Wang and X. Hu, *Adv. Funct. Mater.*, 2022, **32**, 2110653.
13 F. Chen, C. Guo, H. Zhou, M. W. Shahzad, T. X. Liu, S. Oleksandr, J. Sun, S. Dai and B. B. Xu, *Small*, 2022, **18**, e2106352.
14 X. Yang, F. Zhang, L. Zhang, T. Zhang, Y. Huang and Y. Chen, *Adv. Funct. Mater.*, 2013, **23**, 3353–3360.
15 D. Lee, Y. Song, Y. Song, S. J. Oh, U. H. Choi and J. Kim, *Adv. Funct. Mater.*, 2022, **32**, 2109907.
16 J. Zhang, E. Kamio, A. Matsuoka, K. Nakagawa, T. Yoshioka and H. Matsuyama, *Ind. Eng. Chem. Res.*, 2021, **60**, 12640–12649.
17 A. R. Nabais, L. A. Neves and L. C. Tomé, *ACS Appl. Polym. Mater.*, 2022, **4**, 3098–3119.
18 M. G. Cowan, D. L. Gin and R. D. Noble, *Acc. Chem. Res.*, 2016, **49**, 724–732.

19 E. Kamio, M. Minakata, Y. Iida, T. Yasui, A. Matsuoka and H. Matsuyama, *Polym. J.*, 2021, **53**, 137–147.
20 C. Wang, W. Dong, P. Li, Y. Wang, H. Tu, S. Tan, Y. Wu and M. Watanabe, *ACS Appl. Mater. Interfaces*, 2020, **12**, 42202–42209.
21 S. Imaizumi, H. Kokubo and M. Watanabe, *Macromolecules*, 2012, **45**, 401–409.
22 K. Fujii, H. Asai, T. Ueki, T. Sakai, S. Imaizumi, U.-I. Chung, M. Watanabe and M. Shibayama, *Soft Matter*, 2012, **8**, 1756–1759.
23 H. Asai, K. Fujii, T. Ueki, T. Sakai, U.-I. Chung, M. Watanabe, Y.-S. Han, T.-H. Kim and M. Shibayama, *Macromolecules*, 2012, **45**, 3902–3909.
24 Y. Gu, S. Zhang, L. Martinetti, K. H. Lee, L. D. Mcintosh, C. D. Frisbie and T. P. Lodge, *J. Am. Chem. Soc.*, 2013, **135**, 9652–9655.
25 R. Tamate, K. Hashimoto, T. Horii, M. Hirasawa, X. Li, M. Shibayama and M. Watanabe, *Adv. Mater.*, 2018, **30**, 1–7.
26 Y. Kamiyama, R. Tamate, T. Hiroi, S. Samitsu, K. Fujii and T. Ueki, *Sci. Adv.*, 2022, **8**, eadd0226.
27 Y. Kamiyama, R. Tamate, K. Fujii and T. Ueki, *Soft Matter*, 2022, **18**, 8582–8590.
28 M. Wang, P. Zhang, M. Shamsi, J. L. Thelen, W. Qian, V. K. Truong, J. Ma, J. Hu and M. D. Dickey, *Nat. Mater.*, 2022, **21**, 359–365.
29 J. P. Gong, Y. Katsuyama, T. Kurokawa and Y. Osada, *Adv. Mater.*, 2003, **15**, 1155–1158.
30 J. P. Gong, *Soft Matter*, 2010, **6**, 2583–2590.
31 T. Yasui, Y. Zheng, T. Nakajima, E. Kamio, H. Matsuyama and J. P. Gong, *Macromolecules*, 2022, **55**, 9547–9557.
32 Z. Tang, X. Lyu, A. Xiao, Z. Shen and X. Fan, *Chem. Mater.*, 2018, **30**, 7752–7759.
33 D. Weng, F. Xu, X. Li, S. Li, Y. Li and J. Sun, *ACS Appl. Mater. Interfaces*, 2020, **12**, 57477–57485.
34 E. Kamio, T. Yasui, Y. Iida, J. P. Gong and H. Matsuyama, *Adv. Mater.*, 2017, **29**, 1704118.
35 T. Yasui, E. Kamio and H. Matsuyama, *RSC Adv.*, 2020, **10**, 14451–14457.
36 T. Yasui, E. Kamio and H. Matsuyama, *RSC Adv.*, 2019, **9**, 11870–11876.
37 E. Kamio, M. Kinoshita, T. Yasui, T. P. Lodge and H. Matsuyama, *Macromolecules*, 2020, **53**, 8529–8538.
38 T. Watanabe, R. Takahashi and T. Ono, *Soft Matter*, 2020, **16**, 1572–1581.
39 A. Isogai, T. Saito and H. Fukuzumi, *Nanoscale*, 2011, **3**, 71–85.
40 F. Lossada, D. Hoenders, J. Guo, D. Jiao and A. Walther, *Acc. Chem. Res.*, 2020, **53**, 2622–2635.
41 P. Xi, L. Wu, F. Quan, Y. Xia, K. Fang and Y. Jiang, *ACS Appl. Mater. Interfaces*, 2022, **14**, 24787–24797.
42 Y. Jiao, K. Lu, Y. Lu, Y. Yue, X. Xu, H. Xiao, J. Li and J. Han, *Cellulose*, 2021, **28**, 4295–4311.
43 H. Takeno, H. Inoguchi and W.-C. Hsieh, *Mater. Today Commun.*, 2022, **31**, 103495.
44 C. Hopson, M. M. Villar-Chavero, J. C. Domínguez, M. V. Alonso, M. Oliet and F. Rodriguez, *Carbohydr. Polym.*, 2021, **274**, 118663.
45 M. Vranes, S. Dozic, V. Djeric and S. Gadzuric, *J. Chem. Eng. Data*, 2012, **57**, 1072–1077.
46 K. Ueno, K. Hata, T. Katakabe, M. Kondoh and M. Watanabe, *J. Phys. Chem. B*, 2008, **112**, 9013–9019.
47 Y. S. Pek, A. C. A. Wan, A. Shekaran, L. Zhuo and J. Y. Ying, *Nat. Nanotechnol.*, 2008, **3**, 671–675.
48 M. Ognyanov, C. Remoroza, H. A. Schols, Y. N. Georgiev, N. T. Petkova and M. Krystyjan, *Carbohydr. Polym.*, 2020, **229**, 115549.
49 M. A. B. H. Susan, T. Kaneko, A. Noda and M. Watanabe, *J. Am. Chem. Soc.*, 2005, **127**, 4976–4983.
50 E. Kamio, M. Minakata, H. Nakamura, A. Matsuoka and H. Matsuyama, *Soft Matter*, 2022, **18**, 4725–4736.

